Published in final edited form as:

Nat Immunol. 2017 August ; 18(8): 931–939. doi:10.1038/ni.3773.

Runx3 guards cytotoxic CD8+ effector T cells against deviation towards T_{FH} cell lineage

Qiang Shan[1,6], **Zhouhao Zeng**[2,6], **Shaojun Xing**[1], **Fengyin Li**[1], **Stacey M. Hartwig**[1,3], **Jodi A. Gullicksrud**[1,4], **Samarchith P. Kurup**[1], **Natalija Van Braeckel-Budimir**[1], **Yao Su**[5], **Matthew D. Martin**[1,3], **Steven M. Varga**[1,3,4], **Ichiro Taniuchi**[7], **John T. Harty**[1,3,4], **Weiqun Peng**[2,8], **Vladimir P. Badovinac**[1,3,4], and **Hai-Hui Xue**[1,4,8]

[1]Department of Microbiology, University of Iowa, Iowa City, IA 52242

[2]Department of Physics, The George Washington University, Washington DC, 20052

[3]Department of Pathology, Carver College of Medicine, University of Iowa, Iowa City, IA 52242

[4]Interdisciplinary Immunology Graduate Program, University of Iowa, Iowa City, IA 52242

[5]State Key Laboratory of Mycology, Institute of Microbiology, Chinese Academy of Science, Beijing, P. R. China 100101

[7]RIKEN Center for Integrative Medical Sciences, Yokohama, Japan 230-0045

Abstract

Activated $CD8^+$ T cells differentiate into cytotoxic effector (T_{EFF}) cells that eliminate target cells. How T_{EFF} cell identity is established and maintained remains less understood. Here we show Runx3 deficiency limits clonal expansion and impairs upregulation of cytotoxic molecules in T_{EFF} cells. Runx3-deficient $CD8^+$ T_{EFF} cells aberrantly upregulate genes characteristic of follicular helper T (T_{FH}) cell lineage, including *Bcl6*, *Tcf7* and *Cxcr5*. Mechanistically, the Runx3-CBFβ complex deploys H3K27me3 to *Bcl6* and *Tcf7* genes to suppress the T_{FH} program. Ablating *Tcf7* in Runx3-deficient $CD8^+$ T_{EFF} cells prevents the upregulation of T_{FH} genes and ameliorates their defective induction of cytotoxic genes. As such, Runx3-mediated *Tcf7* repression coordinately enforces acquisition of cytotoxic functions and protects the cytotoxic lineage integrity by preventing T_{FH}-lineage deviation.

[8]Corresponding authors: Hai-Hui Xue (Lead Contact), 51 Newton Rd. BSB 3-772, Iowa City, IA 52242, Tel: 319-335-7937, Fax: 319-335-9006, hai-hui-xue@uiowa.edu. Weiqun Peng, Science & Engineering Hall 4790, 800 22nd St NW, Washington, DC 20052, Tel: 202-994-0129, Fax: 202-994-3001, wpeng@gwu.edu.

[6]These authors contributed equally to experimental and systems biology studies, respectively.

Author contribution

Q.S. performed most of the experiments with help of S.X., F.L., S.M.H., J.A.G., S.P.K., N.V.B.B., Y.S., and M.D.M; Z.Z. analyzed the high-throughput data under the supervision of W.P.; S.M.V., I.T., J.T.H., and V.P.B contributed critical reagents and provided scientific insights; H.-H.X. conceived the project and supervised the overall study.

Accession codes

Gene Expression Omnibus: RNA-Seq and ChIP-Seq data have been deposited under accession number GSE81888.

Transcription factors play central roles in establishing and maintaining cell identity during development, homeostasis and response to environmental changes[1]. In the immune system, $CD4^+$ and $CD8^+$ T cells are functionally distinct helper and cytotoxic lineages whose identity is stipulated by distinct transcription factors[2–4]. ThPOK is essential for the $CD4^+$ T lineage choice during development and for maintaining $CD4^+$ T lineage integrity, largely through restraining activation of Runx-CBF complex-dependent transcriptional programs[5,6]. Tcf1 and Lef1, although not required for $CD8^+$ T lineage decision, have critical roles in establishing $CD8^+$ T cell identity through their intrinsic HDAC activity[7,8]. In response to acute infection by intracellular microbes, $CD8^+$ T cells differentiate into dedicated cytotoxic effector cells that eliminate infected target cells in response to acute infection by intracellular pathogens[9–11], while $CD4^+$ T cells give rise to T helper 1 (T_H1), T_H2, T_H17, and T_{FH} cells depending on the nature of pathogens[12,13].

Maintaining the identity of $CD8^+$ T effector (T_{EFF}) cells elicited by acute infections is essential for their cytotoxic capacity. The best-known transcriptional regulators in this regard include T-bet, Eomes and Blimp-1, which are potently induced upon $CD8^+$ T cell activation[14]. Whereas deletion of either T-bet or Eomes alone does not have a pronounced effect, combined deletion of both factors causes aberrant activation of the T_H17 program, including upregulation of Rorγt, along with IL-17A and IL-21[15]. Compound deletion T-bet and Blimp-1 leads to induction of Rorγt and IL-17A in $CD8^+$ T_{EFF} cells[16]. These IL-17-producing, T-bet-Eomes- or T-bet-Blimp-1-deficient $CD8^+$ T_{EFF} cells caused progressive inflammatory and wasting syndrome, highlighting an essential requirement for maintaining the cytotoxic lineage integrity. However, it remains unknown if other T helper subset plasticity is transcriptionally and/or epigenetically suppressed in $CD8^+$ T_{EFF} cells.

The Runx-CBF complex consists of unique DNA-binding α subunits (Runx1, 2 or 3) and the obligatory cofactor CBFβ, which does not bind DNA but stabilizes Runx-DNA interaction[17,18]. Runx1 and Runx3 are predominantly expressed in T lineage cells and have redundant functions in repressing ThPOK expression to ensure generation of $CD8^+$ T cells and *Cd4* gene silencing in $CD8^+$ T cells during thymic development[19,20]. A role of Runx3 in inducing interferon-γ (IFN-γ), perforin and granzyme B expression in activated mature $CD8^+$ T cells was suggested from studies utilizing germline-targeted Runx3-deficient $CD8^+$ T cells responding to *in vitro* stimulation[21,22]. However, the *in vivo* role of the Runx-CBF complex in $CD8^+$ T cell responses remains uncharted. We specifically targeted Runx3 in mature T cells and used *in vivo* infection models to reveal an essential role of Runx3 in guarding $CD8^+$ T_{EFF} cells from deviation to the T_{FH} cell lineage, in addition to inducing the expression of cytotoxic mediators.

Results

Loss of Runx3 impairs $CD8^+$ T_{EFF} cell expansion and function

To address the role of Runx3 in $CD8^+$ T cell responses in a physiological setting of *in vivo* infection, we generated hCD2-Cre^+*Rosa26*GFP*Runx3*$^{FL/FL}$ (*Runx3*$^{-/-}$ hereafter) mice where hCD2-Cre specifically deleted floxed genes in mature T cells[6,23]. Thymic development was similar between *Runx3*$^{-/-}$ mice and littermate controls with the genotypes of *Runx3*$^{+/+}$ or *Runx3*$^{+/-}$ (referred to as wild-type because $CD8^+$ T cells in these genotypes

behaved similarly in all assays, Supplementary Fig. 1a). hCD2-Cre-mediated deletion did not occur in natural killer cells, but was efficient in $CD8^+$ T cells, as indicated by GFP expression (Supplementary Fig. 1b). Deletion of Runx3 protein in *Runx3*$^{-/-}$ $CD8^+$ T cells was confirmed by intracellular staining (Supplementary Fig. 1c). The number of $CD8^+$ T cells in the spleen of *Runx3*$^{-/-}$ mice was reduced by about 40% compared with wild-type mice but did not exhibit derepression of CD4 coreceptor or an aberrant activation phenotype (Supplementary Fig. 1d,e). On day 8 post-infection (8 *dpi*) with the Armstrong strain of lymphocytic choriomeningitis virus (LCMV-Arm), *Runx3*$^{-/-}$ mice had diminished frequency and numbers of LCMV glycoprotein 33–41 (GP33)-specific $CD8^+$ T_{EFF} cells compared with wild-type mice, as detected by GP33-tetramer or GP33 peptide-stimulated IFN-γ production (Fig. 1a). In contrast to effective clearance of the virus in wild-type mice on 8 *dpi*, high titers of LCMV were detected in the livers, spleens and lungs of *Runx3*$^{-/-}$ mice (Fig. 1b). These data suggest an essential requirement for Runx3 in mounting protective $CD8^+$ T cell responses.

We also generated hCD2-Cre$^+$*Rosa26*^{GFP}*Cbfb*$^{fl/fl}$ (*Cbfb*$^{-/-}$ hereafter) mice to ablate CBFβ in peripheral $CD8^+$ T cells (Supplementary Fig. 2a). *Cbfb*$^{-/-}$ mice showed greatly diminished $CD8^+$ T_{EFF} cells in response to LCMV-Arm infection compared with *Cbfb*$^{+/+}$ or *Cbfb*$^{+/-}$ littermate controls, similar to *Runx3*$^{-/-}$ mice (Supplementary Fig. 2b), suggesting that the Runx3-CBFβ complex has a predominant role in $CD8^+$ T cell responses to acute infections, without a strong contribution from the Runx1-CBFβ complex. In addition, in a bacterial infection model using *Listeria monocytogenes* expressing ovalbumin 257–264 (OVA257) and GP33 epitopes (LM-OVA-GP33), *Runx3*$^{-/-}$ mice showed a >4-fold reduction in both OVA- and GP33-specific $CD8^+$ T_{EFF} cells compared with wild-type mice (Supplementary Fig. 2c–e), indicating a requirement for Runx3 in $CD8^+$ T cell responses independent of infection type or epitope.

To control for potential alterations in precursor frequency, we crossed *Runx3*$^{-/-}$ with an MHC I-restricted P14 transgenic TCR that is specific for the LCMV-GP33 epitope. We adoptively transferred 2×10^4 naïve *Runx3*$^{-/-}$ or wild-type (*Runx3*$^{+/+}$ or *Runx3*$^{+/-}$) P14 $CD8^+$ T cells into congenic recipients, followed by infection with LCMV-Arm. *Runx3*$^{-/-}$ P14 $CD8^+$ T_{EFF} cells showed substantial lower clonal expansion than wild-type P14 $CD8^+$ T_{EFF} cells from 5 to 8 *dpi* in the blood and spleen of infected recipient mice (Fig. 1c). Functionally, *Runx3*$^{-/-}$ P14 $CD8^+$ T_{EFF} cells produced less IFN-γ, TNF and IL-2, and showed reduced expression of granzyme B compared with wild-type P14 $CD8^+$ T_{EFF} cells (Fig. 1d). *Runx3*$^{-/-}$ and wild-type P14 $CD8^+$ T_{EFF} cells showed similar capacity to upregulate T-bet and Eomes (Fig. 1e), in contrast to a previous study reporting impaired induction of Eomes in Runx3-deficient $CD8^+$ T cells activated *in vitro*[21]. These data indicate an intrinsic requirement for Runx3 in the clonal expansion and the acquisition of cytotoxic functions in $CD8^+$ T_{EFF} cells.

Runx3 activates the cytotoxic program in $CD8^+$ T_{EFF} cells

We detected more active caspase3 and caspase7 in *Runx3*$^{-/-}$ P14 $CD8^+$ T_{EFF} cells than wild-type cells on 6 and 8 *dpi* (Supplementary Fig. 3a), indicating Runx3-deficient $CD8^+$ T_{EFF} cells are more prone to apoptosis, whereas this effect was less pronounced on 4 *dpi*. To

assess the early impact of Runx3 deficiency on CD8$^+$ T_{EFF} cells while avoiding including a high portion of apoptotic cells, we sort-purified CD45.2$^+$ *Runx3*$^{-/-}$ P14 or wild-type P14 CD8$^+$ T_{EFF} cells on 4 *dpi* from CD45.1$^+$ recipient spleens and performed RNA-Seq. Using the Cuffdiff algorithm at a setting of ≥ 2-fold expression changes and false discovery rate ≤ 0.01, we found 422 genes upregulated and 231 genes downregulated in *Runx3*$^{-/-}$ P14 CD8$^+$ T_{EFF} cells compared with wild-type P14 CD8$^+$ T_{EFF} cells (Fig. 2a,b), some of which (13.2% for down- and 11.4% for up-regulated genes) were previously identified in Runx3-deficient CD8$^+$ T cells activated *in vitro*[22](Supplementary Fig. 3b,c).

Among the downregulated genes, *Runx3*$^{-/-}$ P14 CD8$^+$ T_{EFF} cells showed reduced expression in *Prdm1*, which encodes the transcription factor Blimp-1, a critical regulator of CD8$^+$ T_{EFF} cell differentiation[24,25] (Fig. 2a,b), as well as genes encoding cytotoxic effector molecules, such as *Gzma*, *Gzmb*, *Prf1* and *Fasl*, as validated by quantitative RT-PCR (Fig. 2c) or flow cytometry (Fig. 1d). Among the upregulated genes, *Runx3*$^{-/-}$ P14 CD8$^+$ T_{EFF} cells showed increased expression in *Bcl2l11*, which encodes the pro-apoptotic Bim protein, and many genes associated with the T_{FH} lineage cells, including *Bcl6*, *Maf* and *Tcf7* (encoding Bcl-6, Maf and Tcf1 transcription factors, respectively), *Icos*, *Il6ra* and *Il6st* (encoding ICOS, IL-6Rα and gp130 signaling receptors, respectively), *Cxcr5* and *Il21*[13] (Fig. 2a,b). These data indicate that Runx3 controls a broad transcriptional program including activation of the cytotoxic machinery in CD8$^+$ T_{EFF} cells.

Runx3 suppresses the T_{FH} program in CD8$^+$ T_{EFF} cells

We next investigated the functional relevance of the induced T_{FH} lineage-associated genes in *Runx3*$^{-/-}$ CD8$^+$ T_{EFF} cells during acute viral infection. During 4–8 days after LCMV-Arm infection following adoptive transfer of P14 CD8$^+$ T cells, >35% *Runx3*$^{-/-}$ P14 CD8$^+$ T_{EFF} cells in the spleens were CXCR5$^+$, and these *Runx3*$^{-/-}$ P14 CXCR5$^+$CD8$^+$ T cells were SLAM^{lo} Tcf1^{hi} Bcl-6$^+$, whereas only very few wild-type P14 CD8$^+$ T_{EFF} cells were CXCR5$^+$ (Fig. 3a). *Runx3*$^{-/-}$ P14 CD8$^+$ T_{EFF} cells generated in response to infection by LM-GP33 also contained a CXCR5$^+$ subset (Supplementary Fig. 4a). A T_{FH}-enriched gene set, which contains genes that are expressed ≥ 2 fold higher in wild-type CD4$^+$ T_{FH} cells than T_H1 cells elicited by LCMV-Arm infection was previously defined[23]. GSEA revealed a broad upregulation of T_{FH}-enriched genes in *Runx3*$^{-/-}$ CD8$^+$ T_{EFF} cells compared with wild-type cells (Fig. 3b, Supplementary Fig. 4b).

CXCR5 expression guides CD4$^+$ T_{FH} cells into the B cell follicles. Among CD45.2$^+$ CD8$^+$ T_{EFF} cells elicited by LCMV-Arm infection following adoptive transfer, <1% wild-type P14 CD8$^+$ T_{EFF} cells were detected in the B cell follicles of recipient spleens. In contrast, approximately 10% *Runx3*$^{-/-}$ P14 CD8$^+$ T_{EFF} cells localized in the B cell follicles, in spite of their greatly reduced numbers (Fig. 3c). P14 CD8$^+$ T cells activated by LCMV clone 13 (LCMV-Cl13), which causes chronic infection in mice, became exhausted. Consistent with recent studies[26–28], about 20% of wild-type exhausted P14 CD8$^+$ T cells were CXCR5$^+$ and detected in the B cell follicles; by comparison, *Runx3*$^{-/-}$ exhausted P14 CD8$^+$ T cells showed 2–3 fold increase in the CXCR5$^+$ subset and follicle localization (Supplementary Fig. 4c,d). These data indicate that Runx3 suppresses the induction of a T_{FH} cell transcriptional program in CD8$^+$ T cells in response to diverse activation signals.

Runx3$^{-/-}$ CXCR5^{+}CD8^{+} T cells acquire B cell help function

To test whether *Runx3*$^{-/-}$ CXCR5^{+}CD8^{+} T cells have T_{FH}-like B cell helper functions, we adoptively transferred P14 CD8^{+} T cells into wild-type congenic mice and immunized recipient mice with GP33 peptide conjugated with keyhole limpet hemocyanin (KLH-GP33) in the rear footpads. On day 7 post-immunization, both *Runx3*$^{-/-}$ and wild-type P14 CD8^{+} T cells were activated (Fig. 4a), and the resulting *Runx3*$^{-/-}$ P14 CD8^{+} T_{EFF} cells were diminished in numbers compared with wild-type cells in the draining inguinal lymph node (LN) (Fig. 4b). Whereas about 25% wild-type P14 CD8^{+} T_{EFF} cells in the inguinal LNs elicited by protein immunization were CXCR5^{+}, >70% *Runx3*$^{-/-}$ P14 CD8^{+} T_{EFF} cells exhibited a CXCR5^{+}SLAM^{lo} phenotype (Fig. 4b). Compared with wild-type P14 CXCR5^{+}CD8^{+} T_{EFF} cells, *Runx3*$^{-/-}$ P14 CXCR5^{+}CD8^{+} T_{EFF} cells had higher expression of ICOS and Bcl-6, as well as CD40L, which directly mediates T-B cell interaction (Fig. 4b). In addition, *Runx3*$^{-/-}$ P14 CD8^{+} T_{EFF} cells were about 3-fold more frequently detected in the B cell follicles in inguinal LNs than wild-type P14 CD8^{+} T_{EFF} cells (Fig. 4c).

To specifically address if *Runx3*$^{-/-}$ CXCR5^{+}CD8^{+} T_{EFF} cells can provide B cell help, CD45.2^{+} wild-type or *Runx3*$^{-/-}$P14 CD8^{+} T cells were sort-purified to eliminate contaminating CD4^{+} T cells and adoptively transferred into CD45.1^{+}CD4-Cre^{+}*Bcl6*$^{fl/fl}$ (hereafter *Bcl6*$^{-/-}$) mice, in which the endogenous T_{FH} response is abrogated but B cells are functional, followed by immunization with KLH-GP33. On day 7 post-immunization, serum KLH-specific IgG titers were not significantly different in *Bcl6*$^{-/-}$ mice that were not transferred or transferred with wild-type P14 CD8^{+} T cells (Fig. 4d). On the other hand, *Bcl6*$^{-/-}$ mice that received *Runx3*$^{-/-}$ P14 CD8^{+} T cells showed elevated titers of KLH-specific IgG on day 7 and 21 post-immunization (Fig. 4d, Supplementary Fig. 4e), suggesting *Runx3*$^{-/-}$ CXCR5^{+}CD8^{+} effectors can function as B cell helpers. Of note, *Bcl6*$^{-/-}$ mice transferred with *Runx3*$^{-/-}$ P14 cells did not develop germinal centers (data not shown), indicating that KLH-specific IgG production in these mice was not dependent of germinal centers[29–31]. As a control, SMARTA CD4^{+} T cells, which express an MHC II-restricted TCR specific for LCMV GP61 epitope, adoptively transferred into *Bcl6*$^{-/-}$ recipients and immunized with GP61-conjugated KLH, induced higher titers of KLH-specific IgG in recipient mice than *Bcl6*$^{-/-}$ mice transferred with *Runx3*$^{-/-}$ P14 CD8^{+} T cells (Fig. 4d). To directly compare the expression of key T_{FH} molecules in *Runx3*$^{-/-}$ CD8^{+} T cells and wild-type CD4^{+} T_{FH} cells, we co-transferred *Runx3*$^{-/-}$ P14 CD8^{+} T cells and wild-type SMARTA CD4^{+} T cells into *Bcl6*$^{-/-}$ recipients, followed by immunization with both GP33-KLH and GP61-KLH. On day 7 post-immunization, wild-type CD4^{+} T_{FH} cells showed similar ICOS and CD40L expression as *Runx3*$^{-/-}$ CXCR5^{+}CD8^{+} T_{EFF} cells, but expressed higher CXCR5, Bcl-6 and Tcf1 proteins than the latter (Supplementary Fig. 4f), possibly explaining the more efficient B cell help by wild-type CD4^{+} T_{FH} cells. Together, these results indicate that loss of Runx3 expression confers T_{FH}-like functions to CD8^{+} T_{EFF} cells.

Runx3 deploys H3K27me3 to key T_{FH} gene loci

To define the mechanisms by which the Runx3-CBFβ complex coordinates the repression of the T_{FH} program and activation of the cytotoxic program in CD8^{+} T_{EFF} cells in response to acute infection, we performed CBFβ ChIP-Seq using a CBFβ antiserum[32] in wild-type

KLRG1^{hi}IL-7Rα^{lo} P14 CD8$^+$ T_{EFF} cells sort-purified on day 8 after LCMV-Arm infection. *Cbfb*$^{-/-}$ naïve CD8$^+$ T cells were used as a negative control. Using MACS algorithm with stringent settings (≥ 4 fold enrichment over the negative control, $p<1\times10^{-5}$ and FDR<0.05), we identified 12,981 high-confidence CBFβ binding peaks in CD8$^+$ T_{EFF} cells. Approximately 40% CBFβ peaks were detected in gene promoters, while 23% and 37% were distributed in the gene body or intergenic regions, respectively (Supplementary Fig. 5a). The CBFβ peaks partly overlapped with Runx3 binding peaks previously identified by Runx3 ChIP-Seq in CD8$^+$ T cells activated *in vitro*[22], and *de novo* motif discovery analysis identified a highly enriched Runx binding motif in the CBFβ peaks in both promoters and enhancer-overlapping regions (Supplementary Fig. 5b,c).

To define how the Runx3-CBFβ complex co-opts epigenetic mechanisms for target gene regulation, we performed ChIP-Seq of H3K4me1, H3K4me3, H3K27me3 and H3K27ac histone marks on wild-type and *Runx3*$^{-/-}$ P14 CD8$^+$ T_{EFF} cells sort-purified on day 4 after LCMV-Arm infection. We first mapped the direct association of CBFβ peaks with the Runx-CBF-repressed gene loci, *i.e.*, genes upregulated in *Runx3*$^{-/-}$ over control CD8$^+$ T_{EFF} cells (Supplementary Table 1). The CBFβ peaks within the –5 kb to transcription end site (TES) regions were associated with strong H3K27me3 signals in wild-type P14 CD8$^+$ T_{EFF} cells, while the H3K27me3 marks at the same genomic locations were greatly diminished in *Runx3*$^{-/-}$ P14 CD8$^+$ T_{EFF} cells (Supplementary Fig. 5d). In contrast, CBFβ peaks outside these regions were not marked with strong H3K27me3 in wild-type P14 CD8$^+$ T_{EFF} cells, and the H3K27me3 marks were largely unaffected in *Runx3*$^{-/-}$ P14 CD8$^+$ T_{EFF} cells. On the other hand, H3K4me3 signals at the CBFβ peaks were similar between wild-type and *Runx3*$^{-/-}$ P14 CD8$^+$ T_{EFF} cells (Supplementary Fig. 5d).

We further partitioned CBFβ peaks based on their association with the promoter regions, defined as –1 kb to +1 kb flanking the transcript start sites (TSS). Promoter-associated CBFβ peaks had strong signals of both H3K27me3 and H3K4me3 in wild-type CD8$^+$ T_{EFF} cells (Fig. 5a), indicating a bivalent state. In contrast, these CBFβ peaks showed substantial decrease in H3K27me3, while retaining H3K4me3 in *Runx3*$^{-/-}$ P14 CD8$^+$ T_{EFF} cells (Fig. 5a), suggesting that the poised, bivalent promoters may become actively transcribed without Runx3-mediated repression. Among the 422 Runx3-CBF-repressed genes, 219 promoters showed bivalency in wild-type P14 CD8$^+$ T_{EFF} cells. Forty-eight of these bivalent promoters were marked solely with H3K4me3 in *Runx3*$^{-/-}$ P14 CD8$^+$ T_{EFF} cells, including *Bcl2l11* and key T_{FH} genes such as *Bcl6* and *Tcf7* (Fig. 5b,c and Supplementary Fig. 5e). CBFβ did not bind to *Bcl6* TSS but showed modest enriched binding at a –37 kb regulatory region upstream of *Tcf7* in naïve CD8$^+$ T cells; on the other hand, CBFβ bound strongly to both regions in wild-type P14 CD8$^+$ T_{EFF} cells (Fig. 5d,e). This observation suggests that Runx3-CBFβ can be pre-positioned at critical regulatory regions before antigen encounter and then further stabilize binding to these regions or acquire access to new regulatory elements during CD8$^+$ T_{EFF} cell differentiation. Our data indicate that Runx3-CBFβ deploys H3K27me3 mark to repress its target genes, either through promoters or distal regulatory regions.

Runx3 activates promoters and enhancers of the cytotoxic genes

Runx3 binds to key cytotoxic genes such as *Prf1* and *Gzmb*[21,22]. To validate and expand on the regulatory roles of the Runx3-CBFβ complex in activating the cytotoxic program, we focused on the 231 Runx-CBF-activated gene loci, *i.e.*, genes downregulated in *Runx3*$^{-/-}$ over wild-type P14 CD8^{+} T_{EFF} cells. The CBFβ ChIP-Seq peaks were found in 39 gene promoters in wild-type P14 CD8^{+} T_{EFF} cells, including *Prf1*, *Gzmb* and *Prdm1* (Fig. 6 and Supplementary Table 1). Using the H3K4me1^{hi}H3K4me3$^{neg/lo}$H3K27ac^{hi} H3K27me3$^{neg/lo}$ histone modification signature[33], we mapped active enhancers in wild-type and *Runx3*$^{-/-}$ P14 CD8^{+} T_{EFF} cells. Among the 321 CBFβ peaks found within 50 kb of the Runx-CBF-activated gene loci (but outside promoters) in wild-type P14 CD8^{+} T_{EFF} cells, 72 were associated with 57 active enhancers, which were distributed in 35 genes including *Gzmb*, *Ifng*, *Fasl* and *Gzma* (Fig. 6c, Supplementary Fig. 6a–c and Supplementary Table 1). Clustering analysis showed that 43 active enhancers in wild-type P14 CD8^{+} T_{EFF} cells, including those in *Gzmb* and *Ifng,* remained active in *Runx3*$^{-/-}$ P14 CD8^{+} T_{EFF} cells (Supplementary Fig. 6d), while 14 active enhancers, including those in *Fasl* and *Gzma*, lost H3K27ac and/or gained H3K27me3 in *Runx3*$^{-/-}$ P14 CD8^{+} T_{EFF} cells (Supplementary Fig. 6d), indicating they became inactive. These analyses suggest that Runx3 not only acts through pre-formed enhancers, but also contributes to enhancer activation in select target genes. By ChIP-qPCR Runx3-CBFβ complex was detected in the TSS of *Prf1*, *Gzmb* and *Prdm1* genes, and a –22 kb enhancer upstream of *Gzmb* in wild-type P14 CD8^{+} T_{EFF} cells (Fig. 6a–c). In naïve CD8^{+} T cells, however, CBFβ did not bind to the *Gzmb* TSS or –22 kb enhancer or *Prdm1* TSS, and only showed modest enrichment at the *Prf1* TSS (Fig. 6a–c), indicating that the Runx3-CBFβ complex can be pre-positioned at the promoters of Runx3-CBF-activated genes in naïve CD8^{+} T cells and then further stabilize binding, or can acquire access to new promoters or active enhancers during CD8^{+} T_{EFF} cell differentiation.

Runx3 suppresses Tcf1 to repress the T_{FH} program in T_{EFF} cells

To further define the mechanism by which Runx3 represses the T_{FH} program in CD8^{+} T_{EFF} cells, we focused in Tcf1, which is critical for inducing Bcl-6 and repressing Blimp-1 in CD4^{+} T_{FH} cells[23,34,35]. We adoptively transferred P14 CD8^{+} T cells from *Runx3*$^{-/-}$, hCD2-Cre^{+}*Rosa26*^{GFP}*Tcf7*$^{fl/fl}$ (hereafter *Tcf7*$^{-/-}$), hCD2-Cre^{+}*Rosa26*^{GFP}*Runx3*$^{fl/fl}$*Tcf7*$^{fl/fl}$ (*Runx3*$^{-/-}$*Tcf7*$^{-/-}$) and control (with genotype of *Runx3*$^{+/+}$*Tcf7*$^{+/+}$, *Runx3*$^{+/-}$*Tcf7*$^{+/+}$, *Runx3*$^{+/+}$*Tcf7*$^{+/-}$, or *Runx3*$^{+/-}$*Tcf7*$^{+/-}$, referred to as wild-type because CD8^{+} T cells in these genotypes behaved similarly in all assays) P14 TCR transgenic mice into congenic recipient mice, followed by infection with LCMV-Arm. On 6 *dpi*, unlike control or *Tcf7*$^{-/-}$ P14 CD8^{+} T_{EFF} cells, only *Runx3*$^{-/-}$ P14 CD8^{+} T_{EFF} cells contained a distinct CXCR5^{+}SLAM^{lo}ICOS^{hi} subset, which was completely abrogated in *Runx3*$^{-/-}$*Tcf7*$^{-/-}$ P14 CD8^{+} T_{EFF} cells (Fig. 7a). In addition, the increased *Bcl6* and *Il21* transcripts in *Runx3*$^{-/-}$ P14 CD8^{+} T_{EFF} cells were abolished in *Runx3*$^{-/-}$*Tcf7*$^{-/-}$ cells (Fig. 7b), suggesting that Tcf1 is responsible for inducing the T_{FH} program in CD8^{+} T_{EFF} cells. Furthermore, the induction of CXCR5^{+}SLAM^{lo}ICOS^{hi} CD8^{+} T_{EFF} cells was abrogated when *Runx3*$^{-/-}$*Tcf7*$^{-/-}$ P14 CD8^{+} T cells were activated by LM-GP33, LCMV Cl13 and GP33-KLH immunization (Supplementary Fig. 4a,c and Supplementary Fig. 7a), indicating that Runx3-mediated repression of Tcf1 is a conserved molecular circuit that prevents activation of the T_{FH} program in CD8^{+} T_{EFF} cells activated by diverse stimuli.

Compared with *Runx3*$^{-/-}$ P14 CD8^{+} T_{EFF} cells, *Runx3*$^{-/-}$*Tcf7*$^{-/-}$ P14 CD8^{+} T_{EFF} cells showed about 4-fold increase in clonal expansion on day 6 after LCMV-Arm infection, albeit still lower than wild-type P14 CD8^{+} T_{EFF} cells (Fig. 7c). In addition, the decreased CD25 expression, IFN-γ and granzyme B production observed in *Runx3*$^{-/-}$ P14 CD8^{+} T_{EFF} cells was restored in *Runx3*$^{-/-}$*Tcf7*$^{-/-}$ cells to a level close to wild-type P14 CD8^{+} T_{EFF} cells (Fig. 7d). Further, expression of *Prdm1*, *Fasl* and *Prf1* was higher in *Tcf7*$^{-/-}$*Runx3*$^{-/-}$ P14 CD8^{+} T_{EFF} cells than *Runx3*$^{-/-}$ cells (Fig. 7b), indicating that repression of Tcf1 by Runx3 is intrinsically necessary for Runx3 to fully activate the cytotoxic program and promote clonal expansion of CD8^{+} T_{EFF} cells. Collectively, our data suggest that Runx3 constitutes a key module of the transcriptional network that allows activated CD8^{+} T cells to become cytotoxic effector cells and prevents deviation to helper lineages in response to acute infections (Supplementary Fig. 7b).

Discussion

Using *in vivo* infection models, here we show that Runx3 has a dual function, i.e., activation of the cytotoxic program and repression of the T_{FH} program, during CD8^{+} T cell responses. Differentiation of CD8^{+} T_{EFF} cells is orchestrated by multiple transcriptional and epigenetic regulators[14]. In our recent study mapping transcription factor motifs in active enhancers during CD8^{+} T cell responses, Runx motif is among the most enriched during the transition of naïve to CD8^{+} T_{EFF} cells[36]. Unlike T-bet, Eomes or Blimp-1, which are strongly upregulated during CD8^{+} T_{EFF} cell differentiation, Runx3 is only minimally induced in CD8^{+} T_{EFF} cells compared with naïve CD8^{+} T cells[36,37]. As such, Runx3 appears as a 'housekeeping' factor that acquires regulatory roles in CD8^{+} T_{EFF} cells by gaining access to new regulatory elements (compared with naïve CD8^{+} T cells) and/or cooperate with newly induced factors to achieve stabilized binding to key targets in the cytotoxic program. While being critical for optimal upregulation of Blimp-1 in CD8^{+} T_{EFF} cells, Runx3-CBFβ does not appear to be required for induction of T-bet or Eomes. Whether Runx3 and the T-bet-Eomes pathways act in parallel and/or cooperatively to program CD8^{+} T_{EFF} cell differentiation merits further investigation.

Maintaining the identity of activated CD8^{+} T cells is critical for their dedicated cytotoxic functions[4], as indicated by the combined deficiency of T-bet together with Eomes or Blimp-1, a situation in which CD8^{+} T_{EFF} cells aberrantly produce IL-17 and cause wasting inflammatory diseases[15,16]. Our observations indicate that Runx3 is required for preventing activation of the T_{FH} program in CD8^{+} T_{EFF} cells in response to acute infections. By deploying H3K27me3 repressive mark to T_{FH} cell-associated gene loci, Runx3 thus provides constant supervision of CD8^{+} T_{EFF} cell identity. Because epigenetic spreading of repressive histone marks may differ in individual cells within a population, only a portion of the Runx3-deficient CD8^{+} T_{EFF} cells showed strong upregulation of CXCR5 and Bcl-6. Of note, key gene loci in the T_{FH} lineage, such as *Tcf7* and *Bcl6* were in a bivalent state, decorated with both active and repressive histone marks in wild-type CD8^{+} T_{EFF} cells. This observation suggests that these genes are in a poised status for potential activation, and hence some T cell lineage plasticity is embedded in CD8^{+} T_{EFF} cells. In fact, CD8^{+} T cells have the capacity to produce IL-4 or IL-9 under *in vitro* polarization conditions, at specific anatomical locations or under specific allergic or inflammatory conditions *in vivo*[38]. Thus,

beyond activation of the cytotoxic program, Runx3 might cooperate with other key factors, such as T-bet, Eomes and Blimp-1, to prevent the activation of alternative helper programs in the context of acute infections.

Our results indicate that loss of Tcf1 repression mediates activation of the T_{FH} program in Runx3-deficient $CD8^+$ T_{EFF} cells, and this is consistent with the known role of Tcf1 in promoting $CD4^+$ T_{FH} cell differentiation[23,34,35]. On the other hand, deletion of Tcf1 in *Runx3*$^{-/-}$ $CD8^+$ T_{EFF} cells also improved activation of the cytotoxic program, in particular IFN-γ production and granzyme B expression, and enhanced expression of CD25 and Blimp-1, which may in turn help clonal expansion in response to acute infections. In fact, forced expression of CD25 in *Runx3*$^{-/-}$ $CD8^+$ T_{EFF} cells did improve clonal expansion, albeit showing little effect on increasing IFN-γ and granzyme B production (Q.S. and H.-H. X., unpublished data). These observations indicate that activation of the cytotoxic program and repression of the T_{FH} program are not independent events, but are at least partly interconnected and coordinated by Runx3 and Tcf1. In naïve $CD8^+$ T cells, loss of Tcf1 alone causes upregulation of perforin, granzyme B and Blimp-1 without overt activation signals[8]. Thus, Tcf1 may function as a 'brake' to restrain induction of the cytotoxic program in $CD8^+$ T cells, and this may explain why Tcf1 is strongly downregulated in fully differentiated $CD8^+$ effector T cells[39]. Thus, Runx3-mediated Tcf1 repression is critical for $CD8^+$ T_{EFF} cells to fully acquire cytotoxicity and prevent deviation to the T_{FH} lineage.

During chronic infection, antigen-specific $CD8^+$ T cells initially acquire effector functions but gradually become less functional due to antigen persistence in the hosts[40]. A portion of the exhausted $CD8^+$ T cells have been found to gain T_{FH} cell-like features, including expression of CXCR5, Bcl-6 and Tcf1, with $CXCR5^+CD8^+$ T cells maintaining the pool of exhausted $CD8^+$ T cells and contributing to viral curtailment more than their $CXCR5^-CD8^+$ counterparts[26–28]. Therefore, depending on the context of $CD8^+$ T cell activation, *e.g.,* duration of antigen exposure and cytokine milieu, activation of the T_{FH} program in $CD8^+$ T cells may have beneficial effect. When *Runx3*$^{-/-}$ $CD8^+$ T cells were activated in response to protein immunization, the $CXCR5^+CD8^+$ T_{EFF} cells migrated into the B cell follicles and helped antibody production, and this B cell help function was not accompanied by germinal center formation, consistent with a current view of extrafollicular help to B cells[29–31]. Considering that the expression levels of key T_{FH} factors such as *Bcl6* remained lower in *Runx3*$^{-/-}$ $CD8^+$ T_{EFF} cells than wild-type $CD4^+$ T_{FH} T cells, it is thus not unexpected that the B cell help from the *Runx3*$^{-/-}$ $CXCR5^+CD8^+$ T_{EFF} cells was not as potent as $CD4^+$ T_{FH} cells. Of note, exhausted $CXCR5^+$ or $Tcf1^{hi}$ $CD8^+$ T cells induced by chronic infection express about 60–70% of Runx3 transcripts compared with $CXCR5^-$ or $Tcf1^{lo}$ $CD8^+$ T cells[27,41]. Runx3 may thus represent a novel target, and the resulting T_{FH} plasticity in $CD8^+$ effector T cells may benefit the control of chronic viral infections and/or tumor immunotherapy. Collectively, our study showed that $CD8^+$ T cell identity is under constant supervision both during development and after activation. The underlying regulatory circuits should provide useful tools to prevent unnecessary identity diversion and at the same time confer the plasticity desired.

METHODS

Mice

C57BL/6J (B6), B6.SJL, *Runx3*$^{fl/fl}$, *Cbfb*$^{fl/fl}$, *Bcl6*$^{fl/fl}$, and Rosa26^{GFP} mice were from the Jackson Laboratory. *Tcf7*$^{fl/fl}$ mice were previously described and hCD2-Cre mice were provided by Paul E. Love (NICHD, NIH)[7,23]. All compound mouse strains used in this work were from in-house breeding at the University of Iowa animal care facility. All mice analyzed were 6–12 weeks of age, and both genders are used without randomization or blinding. All mouse experiments were performed under protocols approved by the Institutional Animal Use and Care Committees of the University of Iowa.

Peptide stimulation, active caspase detection, and flow cytometry

Single-cell suspensions were prepared from the spleen, LNs, or peripheral blood, and surface or intracellularly stained as described[39,42]. For analysis at 48–60 hrs and day 4 post-infection, the spleen was first treated with 100 U/ml Collagenase II (Life Technologies) at 37°C for 30 min to maximize cell recovery. The fluorochrome-conjugated antibodies were as follows: anti-CD8 (53-6.7), anti-TCRβ (H57-597), anti-DX5 (DX5), anti-NK1.1 (PK136), anti-Thy1.2 (53-2.1), anti-CD4 (RM4-5), anti-CD44 (IM7), anti-CD62L (MEL-14), anti-CD69 (H1.2F3), anti-CD40L (MR1), anti-CD45.2 (104), anti-ICOS (C398.4A), anti-CD25 (M1/69), anti-IFN-γ (XMG1.2), anti-TNFα (MP6-XT22), anti-Eomes (Dan11mag), anti-T-bet (eBio4B10), and anti-IL-2 (JES6-5H4) from eBiosciences; anti-Bcl6 (K112-91) and anti-Runx3 (R3-5G4) from BD Biosciences; anti-human granzyme B (FGB12) and corresponding isotype control from Invitrogen/Life Technologies, anti-Tcf1 (C63D9) from Cell Signaling Technology; anti-SLAM (TC15-12F12.2) from BioLegend. For detection of CXCR5, three-step staining protocol was used with unconjugated anti-CXCR5 (2G8; BD Biosciences)[23]. For detection of Bcl6 or Tcf1, surface-stained cells were fixed and permeabilized with the Foxp3/Transcription Factor Staining Buffer Set (eBiosciences), followed by incubation with corresponding fluorochrome-conjugated antibodies. GP33- and OVA-specific MHC-I tetramers were generated in-house at the Badovinac lab. Peptide-stimulated cytokine production and detection by intracellular staining were as described[39]. Active Caspsase-3/7 was detected using the Vybrant FAM caspase-3/7 assay kit (Invitrogen/Life Technologies) as described[39]. Data were collected on an LSRII with Violet and a FACSVerse (BD Biosciences) and were analyzed with FlowJo software (TreeStar).

Adoptive transfer and viral or bacterial infection

Naïve P14 CD8$^+$ T cells were isolated from the LNs from WT, *Runx3*$^{-/-}$, *Tcf7*$^{-/-}$, *Runx3*$^{-/-}$*Tcf7*$^{-/-}$ P14 TCR transgenic mice. For characterization of CD8$^+$ effector T cell responses on 4, 6, or 8 *dpi*, 2 × 10^4 Vα2$^+$ P14 CD8$^+$ T cells were intravenously (*i.v.*) injected into CD45.1$^+$ B6.SJL recipient mice and infected intraperitoneally (*i.p*) with 2 × 10^5 PFU of LCMV-Arm, or 2 × 10^6 PFU of LCMV-Cl13. To obtain enough cells for RNA-Seq, ChIP-Seq for histone marks, 2 × 10^5 cells were transferred and P14 CD8$^+$ T_{EFF} cells were sort-purified on 4 *dpi*. For characterization of early CD8$^+$ T cell activation and division within 60 hrs post-infection, P14 CD8$^+$ T cells were labeled with 10 μM Cell Trace Violet (Invitrogen/Life Sciences), and 1×10^6 of labeled cells were transferred followed by *i.v.*

infection with 2×10^6 PFU of LCMV-Arm. In some experiments, *Runx3*$^{-/-}$ or WT mice were directly infected with 2×10^5 PFU of LCMV-Armstrong (*i.p.*) or 5×10^6 CFU of *Listeria monocytogenes* expressing both GP33 and Ovalbumin (OVA) 257 epitopes (LM-GP33-OVA, *i.v.*). Viral titers in the spleen, lung and liver were quantified with standard plaque assay on VERO cells as previously described[43].

Immunization and Enzyme-Linked Immunosorbent Assay (ELISA)

The LCMV GP33-41 peptide (KAVYNFATC) was synthesized and conjugated with KLH to the cysteine by the GenScript. The GP33-KLH conjugates (50 μg/mouse; 25 μg/rear footpad) were mixed with Addavax (Invivogen) at 1:1 volume ratio, then with polyinosine-polycytidylic acid (10 μg/mouse, Sigma-Aldrich) and used as the immunogen. *Runx3*$^{-/-}$ or WT P14 CD8$^+$ T cells were sort-purified to eliminate contamination by CD4$^+$ T cells and adoptively transferred into CD45.1$^+$ B6.SJL or CD45.1$^+$CD4-Cre$^+$*Bcl6*$^{fl/fl}$ (*Bcl6*$^{-/-}$) mice at 1×10^5 cells per recipient. Twenty-four hours later, the recipients were immunized with the immunogen by subcutaneous injection to the rear footpads. Seven days later, the inguinal LNs and spleens were harvested for characterization of activated CD8$^+$ T cells. On days 7 and 21 post-immunization, sera were collected for ELISA, and inguinal LNs harvested for confocal microscopy analysis.

KLH-specific IgG in the sera was measured by ELISA as previously described[44]. In brief, Nunc MaxiSorp flat-bottom 96 well plate (eBiosciences) was coated with 1 μg/ml Imject mcKLH (Thermo Fisher Scientific) overnight, and then incubated with serial diluted serum samples. The KLH-specific IgG was detected by Horseradish peroxidase (HRP)-conjugated goat-anti-mouse IgG (H+L) secondary antibody (Thermo Fisher Scientific) coupled with TMB substrate (BD Biosciences). The absorbance at 450 nm was read on a Synergy H1M microplate reader (BioTek Instruments).

RNA-Seq and data analysis

Total RNA was extracted from *Runx3*$^{-/-}$ or WT CD45.2$^+$GFP$^+$ P14 CD8$^+$ T_{EFF} cells sorted on 4 *dpi* in the adoptive transfer and LCMV-Arm infection experiments, and two biological replicates were obtained for each genotype. RNA-Seq was performed as previously described[23]. The sequencing quality of RNA-seq libraries was assessed by FastQC v0.10.1 (http://www.bioinformatics.babraham.ac.uk/projects/fastqc/). RNA-Seq libraries were mapped to mouse genome using Tophat (v2.1.0)[45], and the mapped reads were then processed by Cuffdiff (v2.2.1)[46] to estimate expression levels of all genes and identify differentially expressed genes. The expression level of a gene is expressed as a gene-level Fragments Per Kilobase of transcripts per Million mapped reads (FPKM) value. The reproducibility of RNA-Seq data was evaluated by computing Pearson's correlation of FPKM values for all genes between biological replicates. The Pearson's correlation coefficient between the two biological replicates was 0.955 for the WT samples, and 0.962 for the *Runx3*$^{-/-}$ samples, indicating strong reproducibility. Upregulated or downregulated genes in *Runx3*$^{-/-}$ CD8$^+$ T cells were identified by requiring ≥ 2-fold expression changes and false discovery rate (FDR) < 0.05, as well as FPKM ≥ 1 in *Runx3*$^{-/-}$ CD8$^+$ T_{EFF} cells for upregulated genes, or FPKM ≥ 1 in control CD8$^+$ T_{EFF} cells for downregulated genes. UCSC genes from the iGenome mouse mm9 assembly (http://support.illumina.com/

sequencing/sequencing_software/igenome.html) were used for gene annotation. The RNAseq data are deposited at the GEO (accession number GSE81888).

Gene set enrichment analysis (GSEA)

GSEA was performed with GSEA software from the Broad Institute[47], and used to determine the enrichment of gene sets in *Runx3*$^{-/-}$ or WT CD8^{+} T_{EFF} cells. T_{FH}-associated gene set was generated in-house based on published results (GEO accession code GSE21380)[23].

ChIP-Seq of histone marks and enhancer analysis

WT or *Runx3*$^{-/-}$ P14 CD8^{+} T_{EFF} cells were sorted from CD45.1^{+} recipient mice on 4 *dpi* in adoptive transfer and LCMV-Arm infection experiments, and used for ChIP-Seq of H3K4me1, H3K4me3, H3K27ac, and H3K27me3 as described[8]. The ChIP-Seq data were processed with SICER (v1.1)[48] to identify islands significantly enriched with each histone mark with the setting of FDR < 10^{-4}. Active enhancers were defined as H3K4me1^{hi} H3K4me3$^{neg/lo}$ H3K27ac^{lo} H3K27me3$^{neg/lo}$ regions that located 1 kb away from transcriptional start sites (TSS). Specifically, the H3K4me1 islands were first identified, and then any portion(s) that overlap with H3K4me3 islands were removed. The resulting H3K4me1^{hi} H3K4me3$^{neg/lo}$ regions were then compared with gene promoters (defined as –1 kb to + 1 kb regions flanking the TSS), and further modified as follows: 1) if more than half of an H3K4me1^{hi} H3K4me3$^{neg/lo}$ − region overlapped with a gene promoter, this region was removed in its entirety, and 2) if the overlap was less than half of the length of the H3K4me1^{hi} H3K4me3$^{neg/lo}$ region, the overlapping portion was removed from the region. Further overlay with H3K27ac and H3K27me3 islands thus identified gene promoter-excluded H3K4me1^{hi} H3K4me3$^{neg/lo}$ H3K27ac^{lo} H3K27me3$^{neg/lo}$ regions, which were considered as active enhancers. During the data processing outlined above, internal truncation and/or trimming of disqualified genomic regions may have generated short fragments that retained the required histone mark features, and any fragments < 500 bp were excluded from the active enhancer repertoire. The histone mark ChIP-Seq data are also under GEO accession number GSE81888.

ChIP-Seq of CBFβ in CD8^{+} T_{EFF} cells and data processing

hCD2-Cre^{+}Rosa26^{GFP}*Cbfb*$^{FL/FL}$ (*Cbfb*$^{-/-}$) naïve CD8^{+} T cells were isolated by negative selection from uninfected mice. CD45.2^{+}KLRG1^{hi}IL-7Rα^{lo} CD8^{+} T_{EFF} cells were sorted from CD45.1^{+} recipient mice on 8 *dpi* in adoptive transfer and LCMV-Arm infection experiments. The cells were incubated with 2 mM disuccinimidyl glutarate (DSG, Sigma Aldrich) at room temperature for 45 min, and then cross-linked for 10 min with 1% formaldehyde in medium. The fixed cells were processed with a truChIP Chromatin Shearing Reagent Kit (Covaris) and sonicated for 5 min on Covaris S2 ultrasonicator. The sheared chromatin from 3–5 × 10^{6} CD8^{+} T cells was immunoprecipitated with 5 μg of purified anti-CBFβ antibody[32] and was washed as described[23]. DNA segments from ChIP were end-repaired and ligated to indexed Illumina adaptors followed by low-cycle PCR. The resulting libraries were sequenced with the Illumina HiSeq-2000 platform.

The sequencing quality of ChIP-Seq libraries was assessed by FastQC. Bowtie2 v2.2.6[49] was used to align the sequencing reads to the mm9 mouse genome. UCSC genes from the iGenome mouse mm9 assembly were used for gene annotation. MACS v1.4.2[50] was used for peak calling with CBFβ ChIP-Seq in *Cbfb*$^{-/-}$ CD8^{+} T cells as a negative control. We used a stringent setting, *i.e.*, ≥ 4 fold enrichment, p-value < 10^{-5}, and FDR < 5%, and identified 12,981 high-confidence CBFβ binding peaks in CD8^{+} T_{EFF} cells.

To determine the overlap of CBFβ binding peaks with active enhancers, CBFβ binding peaks were compared with active enhancers defined above, and at least one base pair overlap was required to consider potential direct association of CBFβ with an active enhancer. To determine the overlap of CBFβ binding peaks with Runx3 binding peaks, the Runx3 ChIP-Seq data were retrieved from GSE50131[22] and processed using the same protocol and stringent setting as above. At least one base pair overlap was required to consider a CBFβ peak and a Runx3 peak overlap with each other.

The profile of a histone mark flanking the CBFβ binding peaks in CD8^{+} T_{EFF} cells was generated as follows. The CBFβ peaks were aligned by their summits, and the island-filtered reads of the histone mark were counted in a resolution of 100 bps and with smoothing window of 400 bps within ±5 kb region flanking the summits. The read counts in each window were then normalized by the number of CBFβ peaks and by the window size, and expressed as reads per kb. The profile was further normalized by the total number of island-filtered reads in the histone mark library as reads per kilobase per million reads (RPKM). The CBFβ ChIP-Seq data are also under GEO accession number GSE81888.

De novo motif analysis

Among the 12,981 high-confidence CBFβ peaks in CD8^{+} T_{EFF} cells, 5,186 were at the promoter region, and 1,758 overlapped with the putative enhancers (defined as H3K4Me1^{hi} H3K4Me3$^{neg/lo}$ regions that are located with 5 kbs of TSS). The top 3,000 most significant CBFβ peaks at the promoters as ordered by *p*-value and all CBFβ peaks overlapping with the putative enhancers were used for motif analysis. The sequences of ± 200 bps flanking the peak summits, as identified by MACS, were used in MEME-ChIP for *de novo* motif discovery[51].

Immunohistochemistry

Fresh spleens or LNs were snap-frozen in Tissue-Tek optimum cutting temperature (O.C.T.) compound (Sakura Finetek). Cryosections of 10 μm were cut, fixed in 4% of paraformaldehyde for 10 min followed by another 10 min incubation in pre-chilled acetone at −20 °C, and then washed three times with PBS for immunostaining. Following incubation in blocking buffer (CAS-Block, Invitrogen), the samples were incubated with fluorescence-labeled antibodies overnight at 4 °C. The primary antibodies used are anti-mouse CD8-Alexa Fluor 594 (53-6.7), anti-mouse B220-BV510 or B220-Alexa Fluor 647 (RA3-6B2 for both fluorochromes), and anti-mouse CD45.2-Alexa Fluor 488 (clone 104, all from BioLegend). Confocal images of cryosections were acquired using a Zeiss LSM710 confocal fluorescence microscopy and were processed with Imaris software (Bitplane).

Chromatin immunoprecipitation (ChIP)

hCD2-Cre^{+}Rosa26^{GFP}*Cbfb*$^{FL/FL}$ (*Cbfb*$^{-/-}$) or WT naïve CD8^{+} T cells were isolated by negative selection from uninfected mice. P14 CD8^{+} T_{EFF} cells were sorted from CD45.1^{+} recipient mice on 5 *dpi* in adoptive transfer and LCMV-Arm infection experiments. The purified cells were cross-linked for 10 min with 1% formaldehyde in medium, were processed with a truChIP Chromatin Shearing Reagent Kit (Covaris) and sonicated for 5 min on Covaris S2 ultrasonicator. The sheared chromatin from 3–5 × 10^6 CD8^{+} cells was immunoprecipitated with 5 μg of purified anti-CBF-β antibody[32] or control rabbit IgG and was washed as described[23]. The immunoprecipitated DNA segments were used for quantification by PCR. For calculation of enriched binding by CBF-β, the signal at the genomic region of interest in each ChIP sample were first normalized to that at the *Hprt* promoter, and the enrichment by anti-CBF-β was then normalized to that by IgG in corresponding ChIP sample.

The primers used for ChIP-PCR are:

Prf1 TSS, 5′-agcactgcaccatgtcttca and 5′-atgcgctgtcaggaagagtt;

Gzmb TSS, 5′-taaccacagcagaacccaca and 5′-tccaaaacactgatgctcca;

Gzmb –22 kb enhancer, 5′-ccacctctagcagcacttcc and 5′-tgagcctctgtcatctgtgg;

Prdm1 TSS, 5′-ctgccgcagacttctttacc and 5′-tttgcaaacagaggaagctg;

Bcl6 TSS, 5′-ggcagcaacagcaataatca and 5′-ctgcggagcaatggtaaag;

Tcf7 –37 kb region, 5′-tttctgctccccactcaaac and 5′-ttcctgaggtgacccatttc;

Hprt TSS, 5′-tgagcgcaagttgaatctg and 5′-ggacgcagcaactgacatt.

Quantitative RT-PCR

P14 CD8^{+} T_{EFF} cells were sorted from recipient mice in adoptive transfer and LCMV-Arm infection experiments. Total RNA was extracted, reverse-transcribed, and target gene transcripts were measured with quantitative PCR as described[7]. The primers used are as follows:

Prdm1, 5′-cctgccaaccaggaacttct and 5′-gttgctttccgtttgtgtgaga;

Prf1, 5′-gatgtgaaccctaggccaga and 5′-ggtttttgtaccaggcgaaa;

Fasl, 5′-gcagaaggaactggcagaac and 5′-ttaaatgggccacactcctc;

Tcf7, 5′-caatctgctcatgccctacc and 5′-cttgcttctggctgatgtcc;

Bcl6, 5′-cctgagggaaggcaatatca and 5′-cggctgttcaggaactcttc;

Actb, 5′-cggttccgatgccctgaggctctt and 5′-cgtcacacttcatgatggaattga.

Statistical analysis

For comparison between two experimental groups, Student’s t-test was used. For multiple group comparison, one way ANOVA was used to first determine whether any of the differences between the means are statistically significant, followed by 1) unpaired Student’s

t-test to determine the statistical significance for a specific pair, 2) post hoc tests using Tukey's test and Bonferroni's test to more stringently determine the statistical significance of differences between all possible pairs[52]. In Fig. 4d, the SMARTA $CD4^+$ T cell recipient group was included as a positive control for the experimental system and was not included in the multi-group comparisons so as not to artificially reduce the statistical power of comparison among $CD8^+$ T cell recipient groups. For comparison of numbers wild-type, *Runx3*$^{-/-}$, *Tcf7*$^{-/-}$, *Runx3*$^{-/-}$ *Tcf7*$^{-/-}$ P14 $CD8^+$ T_{EFF} cells in response to various challenges, the values were log10 transformed for post hoc tests because the numbers of *Runx3*$^{-/-}$ $CD8^+$ T_{EFF} cells were 1–2 logs lower than those of wild-type cells. Both unpaired *t*-test and post hoc tests yielded consistent outcomes, although statistical power differed in some cases. In figures, the level of statistical significance was marked based on the most stringent Bonferroni's test, and that by unpaired t-test and Tukey's test was provided in the "Source data-ANOVA/post-host test" file.

Data Availability

High throughput sequencing data are deposited at the GEO with accession number GSE81888. Experimental protocols are described above or in cited references, and more details can be provided upon requests.

Supplementary Material

Refer to Web version on PubMed Central for supplementary material.

Acknowledgments

We thank J. Fishbaugh, H. Vignes and M. Shey (University of Iowa Flow Cytometry Core Facility) for cell sorting, J. Bair and E. Snir (Genomics Division, Iowa Institute of Human Genetics) for ChIP-Seq, J. Shao (University of Iowa Central Microscopy Research Facility) for assistance with immunofluorescence staining, I. Antoshechkin (California Institute of Technology) for RNA-Seq, S. Crotty (La Jolla Institute) for sharing the protein immunization protocol, W. Chen (Beijing Institute of Genomics) for help with RNA-Seq data analysis and Y. Groner (Weizmann Institute of Science, Israel) for sharing high-throughput data on Runx3. This study is supported by grants from the NIH (AI112579 and AI115149 to H.-H.X., AI119160 to H.-H.X. and V.P.B., AI042767 to J.T.H., AI114543 and GM113961 to V.P.B., AI121080 to H.-H.X. and W.P., AI113806 to W.P.) and the US Department of Veteran Affairs (I01 BX002903 to H.-H.X.). The flow cytometry core facility at the University of Iowa is supported by the Carver College of Medicine, Holden Comprehensive Cancer Center, and Iowa City Veteran's Administration Medical Center, and also by grants from the NCI (P30CA086862) and the National Center for Research Resources of the NIH (S10 OD016199). M.D.M. is supported by a T32 Post-doctoral Training Grant (4T32AI007260-30). JAG is a recipient of the Ballard and Seashore Dissertation Fellowship. The authors declare no conflict of interests.

References

1. Natoli G. Maintaining cell identity through global control of genomic organization. Immunity. 2010; 33:12–24. DOI: 10.1016/j.immuni.2010.07.006 [PubMed: 20643336]
2. Steinke FC, Xue HH. From inception to output, Tcf1 and Lef1 safeguard development of T cells and innate immune cells. Immunol Res. 2014; 59:45–55. DOI: 10.1007/s12026-014-8545-9 [PubMed: 24847765]
3. Taniuchi I, Ellmeier W. Transcriptional and epigenetic regulation of CD4/CD8 lineage choice. Adv Immunol. 2011; 110:71–110. DOI: 10.1016/B978-0-12-387663-8.00003-X [PubMed: 21762816]
4. Gullicksrud JA, Shan Q, Xue HH. Front Biol. 2017

5. He X, Park K, Kappes DJ. The role of ThPOK in control of CD4/CD8 lineage commitment. Annu Rev Immunol. 2010; 28:295–320. DOI: 10.1146/annurev.immunol.25.022106.141715 [PubMed: 20307210]
6. Vacchio MS, et al. A ThPOK-LRF transcriptional node maintains the integrity and effector potential of post-thymic CD4+ T cells. Nature immunology. 2014; 15:947–956. DOI: 10.1038/ni.2960 [PubMed: 25129370]
7. Steinke FC, et al. TCF-1 and LEF-1 act upstream of Th-POK to promote the CD4(+) T cell fate and interact with Runx3 to silence Cd4 in CD8(+) T cells. Nature immunology. 2014; 15:646–656. DOI: 10.1038/ni.2897 [PubMed: 24836425]
8. Xing S, et al. Tcf1 and Lef1 transcription factors establish CD8(+) T cell identity through intrinsic HDAC activity. Nature immunology. 2016; 17:695–703. DOI: 10.1038/ni.3456 [PubMed: 27111144]
9. Harty JT, Badovinac VP. Shaping and reshaping CD8+ T-cell memory. Nat Rev Immunol. 2008; 8:107–119. DOI: 10.1038/nri2251 [PubMed: 18219309]
10. Kaech SM, Wherry EJ. Heterogeneity and cell-fate decisions in effector and memory CD8+ T cell differentiation during viral infection. Immunity. 2007; 27:393–405. DOI: 10.1016/j.immuni.2007.08.007 [PubMed: 17892848]
11. Chang JT, Wherry EJ, Goldrath AW. Molecular regulation of effector and memory T cell differentiation. Nature immunology. 2014; 15:1104–1115. DOI: 10.1038/ni.3031 [PubMed: 25396352]
12. Zhu J, Yamane H, Paul WE. Differentiation of effector CD4 T cell populations (*). Annu Rev Immunol. 2010; 28:445–489. DOI: 10.1146/annurev-immunol-030409-101212 [PubMed: 20192806]
13. Crotty S. T follicular helper cell differentiation, function, and roles in disease. Immunity. 2014; 41:529–542. DOI: 10.1016/j.immuni.2014.10.004 [PubMed: 25367570]
14. Kaech SM, Cui W. Transcriptional control of effector and memory CD8+ T cell differentiation. Nat Rev Immunol. 2012; 12:749–761. DOI: 10.1038/nri3307 [PubMed: 23080391]
15. Intlekofer AM, et al. Anomalous type 17 response to viral infection by CD8+ T cells lacking T-bet and eomesodermin. Science. 2008; 321:408–411. DOI: 10.1126/science.1159806 [PubMed: 18635804]
16. Xin A, et al. A molecular threshold for effector CD8(+) T cell differentiation controlled by transcription factors Blimp-1 and T-bet. Nature immunology. 2016; 17:422–432. DOI: 10.1038/ni.3410 [PubMed: 26950239]
17. Collins A, Littman DR, Taniuchi I. RUNX proteins in transcription factor networks that regulate T-cell lineage choice. Nat Rev Immunol. 2009; 9:106–115. DOI: 10.1038/nri2489 [PubMed: 19165227]
18. Djuretic IM, Cruz-Guilloty F, Rao A. Regulation of gene expression in peripheral T cells by Runx transcription factors. Adv Immunol. 2009; 104:1–23. DOI: 10.1016/S0065-2776(08)04001-7 [PubMed: 20457114]
19. Setoguchi R, et al. Repression of the transcription factor Th-POK by Runx complexes in cytotoxic T cell development. Science. 2008; 319:822–825. DOI: 10.1126/science.1151844 [PubMed: 18258917]
20. Egawa T, Tillman RE, Naoe Y, Taniuchi I, Littman DR. The role of the Runx transcription factors in thymocyte differentiation and in homeostasis of naive T cells. The Journal of experimental medicine. 2007; 204:1945–1957. DOI: 10.1084/jem.20070133 [PubMed: 17646406]
21. Cruz-Guilloty F, et al. Runx3 and T-box proteins cooperate to establish the transcriptional program of effector CTLs. The Journal of experimental medicine. 2009; 206:51–59. DOI: 10.1084/jem.20081242 [PubMed: 19139168]
22. Lotem J, et al. Runx3-mediated transcriptional program in cytotoxic lymphocytes. PLoS One. 2013; 8:e80467. [PubMed: 24236182]
23. Choi YS, et al. LEF-1 and TCF-1 orchestrate T(FH) differentiation by regulating differentiation circuits upstream of the transcriptional repressor Bcl6. Nature immunology. 2015; 16:980–990. DOI: 10.1038/ni.3226 [PubMed: 26214741]

24. Kallies A, et al. Transcriptional repressor Blimp-1 is essential for T cell homeostasis and self-tolerance. Nature immunology. 2006; 7:466–474. DOI: 10.1038/ni1321 [PubMed: 16565720]
25. Rutishauser RL, et al. Transcriptional repressor Blimp-1 promotes CD8(+) T cell terminal differentiation and represses the acquisition of central memory T cell properties. Immunity. 2009; 31:296–308. DOI: 10.1016/j.immuni.2009.05.014 [PubMed: 19664941]
26. He R, et al. Follicular CXCR5-expressing CD8+ T cells curtail chronic viral infection. Nature. 2016; 537:412–428. DOI: 10.1038/nature19317 [PubMed: 27501245]
27. Im SJ, et al. Defining CD8+ T cells that provide the proliferative burst after PD-1 therapy. Nature. 2016; 537:417–421. DOI: 10.1038/nature19330 [PubMed: 27501248]
28. Leong YA, et al. CXCR5(+) follicular cytotoxic T cells control viral infection in B cell follicles. Nature immunology. 2016; 17:1187–1196. DOI: 10.1038/ni.3543 [PubMed: 27487330]
29. Taylor JJ, Jenkins MK, Pape KA. Heterogeneity in the differentiation and function of memory B cells. Trends Immunol. 2012; 33:590–597. DOI: 10.1016/j.it.2012.07.005 [PubMed: 22920843]
30. Tarlinton D, Good-Jacobson K. Diversity among memory B cells: origin, consequences, and utility. Science. 2013; 341:1205–1211. DOI: 10.1126/science.1241146 [PubMed: 24031013]
31. Miyauchi K, et al. Protective neutralizing influenza antibody response in the absence of T follicular helper cells. Nature immunology. 2016; 17:1447–1458. DOI: 10.1038/ni.3563 [PubMed: 27798619]
32. Naoe Y, et al. Repression of interleukin-4 in T helper type 1 cells by Runx/Cbf beta binding to the Il4 silencer. The Journal of experimental medicine. 2007; 204:1749–1755. DOI: 10.1084/jem.20062456 [PubMed: 17646405]
33. Heintzman ND, et al. Histone modifications at human enhancers reflect global cell-type-specific gene expression. Nature. 2009; 459:108–112. DOI: 10.1038/nature07829 [PubMed: 19295514]
34. Wu T, et al. TCF1 Is Required for the T Follicular Helper Cell Response to Viral Infection. Cell Rep. 2015; 12:2099–2110. DOI: 10.1016/j.celrep.2015.08.049 [PubMed: 26365183]
35. Xu L, et al. The transcription factor TCF-1 initiates the differentiation of T(FH) cells during acute viral infection. Nature immunology. 2015; 16:991–999. DOI: 10.1038/ni.3229 [PubMed: 26214740]
36. He B, et al. CD8+ T Cells Utilize Highly Dynamic Enhancer Repertoires and Regulatory Circuitry in Response to Infections. Immunity. 2016; 45:1341–1354. DOI: 10.1016/j.immuni.2016.11.009 [PubMed: 27986453]
37. Best JA, et al. Transcriptional insights into the CD8(+) T cell response to infection and memory T cell formation. Nature immunology. 2013; 14:404–412. DOI: 10.1038/ni.2536 [PubMed: 23396170]
38. Mittrucker HW, Visekruna A, Huber M. Heterogeneity in the differentiation and function of CD8(+) T cells. Arch Immunol Ther Exp (Warsz). 2014; 62:449–458. DOI: 10.1007/s00005-014-0293-y [PubMed: 24879097]
39. Zhao DM, et al. Constitutive activation of Wnt signaling favors generation of memory CD8 T cells. J Immunol. 2010; 184:1191–1199. DOI: 10.4049/jimmunol.0901199 [PubMed: 20026746]
40. Wherry EJ, Kurachi M. Molecular and cellular insights into T cell exhaustion. Nat Rev Immunol. 2015; 15:486–499. DOI: 10.1038/nri3862 [PubMed: 26205583]
41. Utzschneider DT, et al. T Cell Factor 1-Expressing Memory-like CD8(+) T Cells Sustain the Immune Response to Chronic Viral Infections. Immunity. 2016; 45:415–427. DOI: 10.1016/j.immuni.2016.07.021 [PubMed: 27533016]
42. Zhou X, et al. Differentiation and persistence of memory CD8(+) T cells depend on T cell factor 1. Immunity. 2010; 33:229–240. DOI: 10.1016/j.immuni.2010.08.002 [PubMed: 20727791]
43. Shen H, et al. Compartmentalization of bacterial antigens: differential effects on priming of CD8 T cells and protective immunity. Cell. 1998; 92:535–545. [PubMed: 9491894]
44. Jing X, Zhao DM, Waldschmidt TJ, Xue HH. GABPbeta2 is dispensible for normal lymphocyte development but moderately affects B cell responses. J Biol Chem. 2008; 283:24326–24333. DOI: 10.1074/jbc.M804487200 [PubMed: 18628204]
45. Trapnell C, Pachter L, Salzberg SL. TopHat: discovering splice junctions with RNA-Seq. Bioinformatics. 2009; 25:1105–1111. DOI: 10.1093/bioinformatics/btp120 [PubMed: 19289445]

46. Trapnell C, et al. Transcript assembly and quantification by RNA-Seq reveals unannotated transcripts and isoform switching during cell differentiation. Nat Biotechnol. 2010; 28:511–515. DOI: 10.1038/nbt.1621 [PubMed: 20436464]

47. Subramanian A, et al. Gene set enrichment analysis: a knowledge-based approach for interpreting genome-wide expression profiles. Proceedings of the National Academy of Sciences of the United States of America. 2005; 102:15545–15550. DOI: 10.1073/pnas.0506580102 [PubMed: 16199517]

48. Zang C, et al. A clustering approach for identification of enriched domains from histone modification ChIP-Seq data. Bioinformatics. 2009; 25:1952–1958. DOI: 10.1093/bioinformatics/btp340 [PubMed: 19505939]

49. Langmead B. Aligning short sequencing reads with Bowtie. Curr Protoc Bioinformatics. 2010; Chapter 11(Unit 11):17.

50. Zhang Y, et al. Model-based analysis of ChIP-Seq (MACS). Genome Biol. 2008; 9:R137. gb-2008-9-9-r137 [pii]. [PubMed: 18798982]

51. Bailey TL, et al. MEME SUITE: tools for motif discovery and searching. Nucleic Acids Res. 2009; 37:W202–208. DOI: 10.1093/nar/gkp335 [PubMed: 19458158]

52. Lamb TJ, Graham AL, Petrie A. T testing the immune system. Immunity. 2008; 28:288–292. DOI: 10.1016/j.immuni.2008.02.003 [PubMed: 18341999]

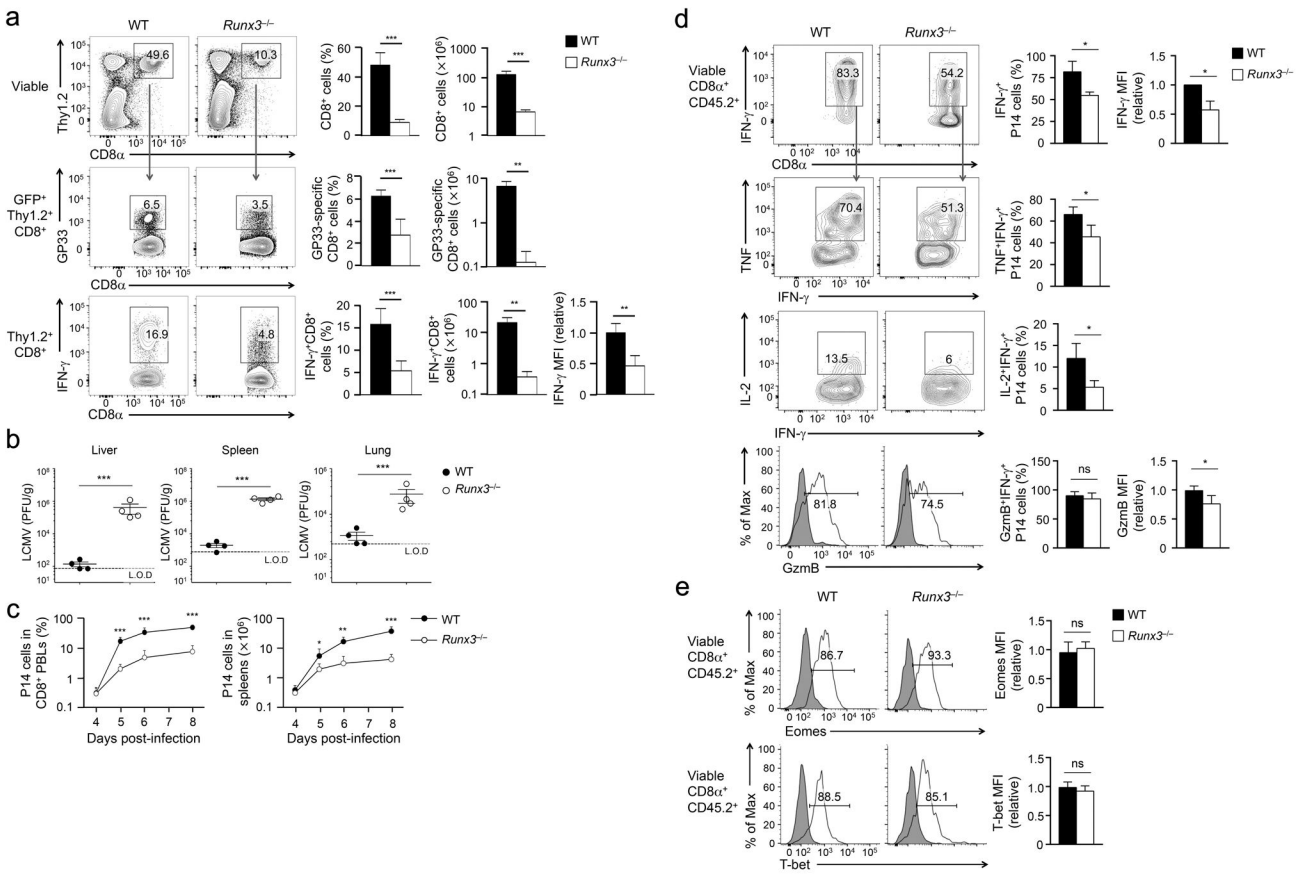

Figure 1. Runx3 is essential for clonal expansion and cytotoxic functions in CD8$^+$ T_{EFF} cells

(**a**) Frequency and numbers of total (top) or antigen-specific (middle, bottom) Thy1.2$^+$CD8$^+$ T_{EFF} cells determined by either GP33 tetramer (middle) or GP33 peptide-stimulated IFN-γ production (bottom) in splenocytes from *Runx3*$^{-/-}$ or wild-type (WT) mice infected with LCMV-Arm on day 8 post-infection. (**b**) Titers of LCMV in the liver, spleen and lung in *Runx3*$^{-/-}$ or WT mice infected with LCMV-Arm on day 8 post-infection. L.O.D., limit of detection. (**c**) Frequency and numbers of P14 CD8$^+$ T_{EFF} cells determined in the peripheral blood lymphocytes (PBLs, left) and the spleens (right), respectively, during days 4–8 post-infection after naïve *Runx3*$^{-/-}$ or WT P14 CD8$^+$ T cells were adoptively transferred into congenic recipients followed by LCMV-Arm infection. (**d**) IFN-γ, TNF, IL-2 and granzyme B (GzmB) expression detected by intracellular staining in GP33 peptide-stimulated splenic *Runx3*$^{-/-}$ or WT P14 CD8$^+$ T_{EFF} cells on day 5 post-infection. (**e**) T-bet and Eomes expression detected by intranuclear staining in splenic *Runx3*$^{-/-}$ or WT P14 CD8$^+$ T_{EFF} cells on day 5 post-infection, with shaded areas denote corresponding isotype controls. Cumulative data in (**a**), (**c**–**e**) are means ± s.d. (n = 3–6) from 3 independent experiments. *, p<0.05; **, p<0.01; ***, p<0.001 (Student's *t*-test), and data in (**b**) are from 2 experiments.

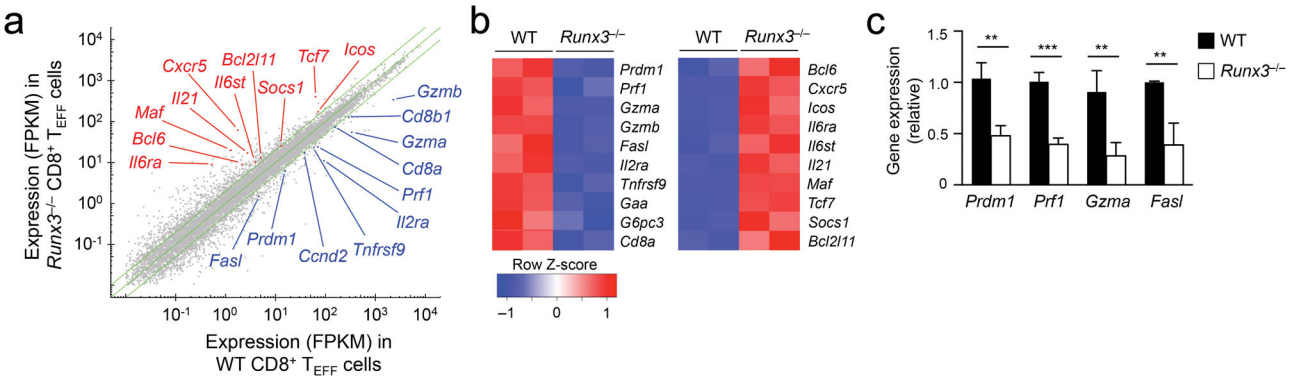

Figure 2. Runx3 activates the cytotoxic program in CD8$^+$ T$_{EFF}$ cells

(**a**) RNA-Seq analysis of *Runx3*$^{-/-}$ or WT P14 CD8$^+$ T$_{EFF}$ cells sort-purified from the spleen on day 4 after adoptive transfer and LCMV-Arm infection. Shown are scatterplot of the average fragments per kilobase of transcripts per million mapped reads (FPKM) values of two replicates of WT *vs.* *Runx3*$^{-/-}$P14 T$_{EFF}$ cells are shown, with green lines denoting gene expression changes by a factor of 2. (**b**) Heatmap showing select downregulated (left) or upregulated (right) genes in *Runx3*$^{-/-}$ P14 T$_{EFF}$ cells. (**c**) qRT-PCR analysis of *Prdm1*, *Prf1*, *Fasl* and *Gzma* expression (relative to the *Hprt* housekeeping gene) in WT or *Runx3*$^{-/-}$ P14 T$_{EFF}$ cells sorted from the recipient spleens on day 4 after adoptive transfer and LCMV-Arm infection. Data are means ± s.d. (n = 4) from 2 independent experiments. **, p<0.01; ***, p<0.001 (Student's *t*-test).

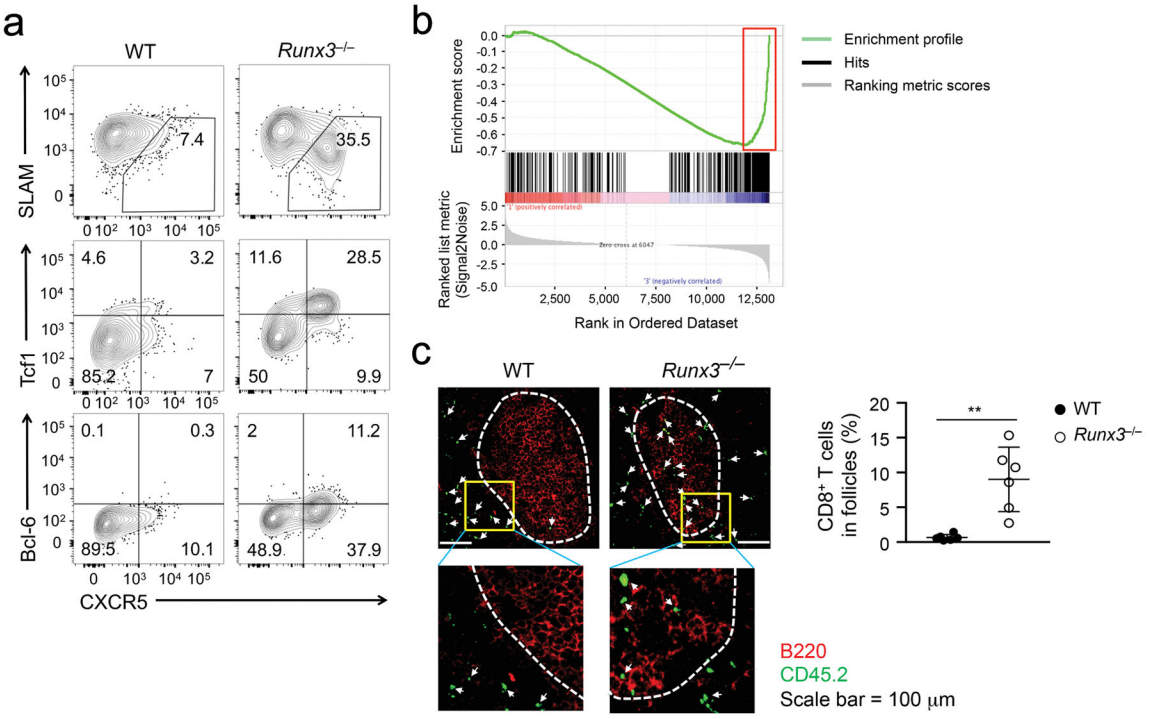

Figure 3. Runx3 represses T_{FH}-associated genes in CD8$^+$ T_{EFF} cells

(**a**) Expression of CXCR5, SLAM, Tcf1 and Bcl-6 detected by surface or intracellular staining in WT or *Runx3*$^{-/-}$ P14 CD8$^+$ T_{EFF} cells in spleen on day 6 after adoptive transfer and LCMV-Arm infection. Data are representative from 3 independent experiments. (**b**) GSEA enrichment plot showing the enrichment of T_{FH}-associated gene set in *Runx3*$^{-/-}$ P14 T_{EFF} cells, as highlighted in a red rectangle. (**c**) Immunofluorescence staining of distribution of CD45.2$^+$ WT or *Runx3*$^{-/-}$ P14 T_{EFF} cells (green) in B cell (red) follicles in spleen sections on day 8 after adoptive transfer and LCMV-Arm infection. Lower panels are 9-fold enlargement of highlighted areas outlined in the main images, and white dotted lines denote the boundary of B cell follicles and T cell zone. The frequency of CD45.2$^+$CD8$^+$ T cells in B cell follicles among all CD45.2$^+$ cells in the scanned images is shown in dot plots, with each dot representing one recipient mouse (pooled from 2 independent experiments). **, $p<0.01$ (Student's *t*-test).

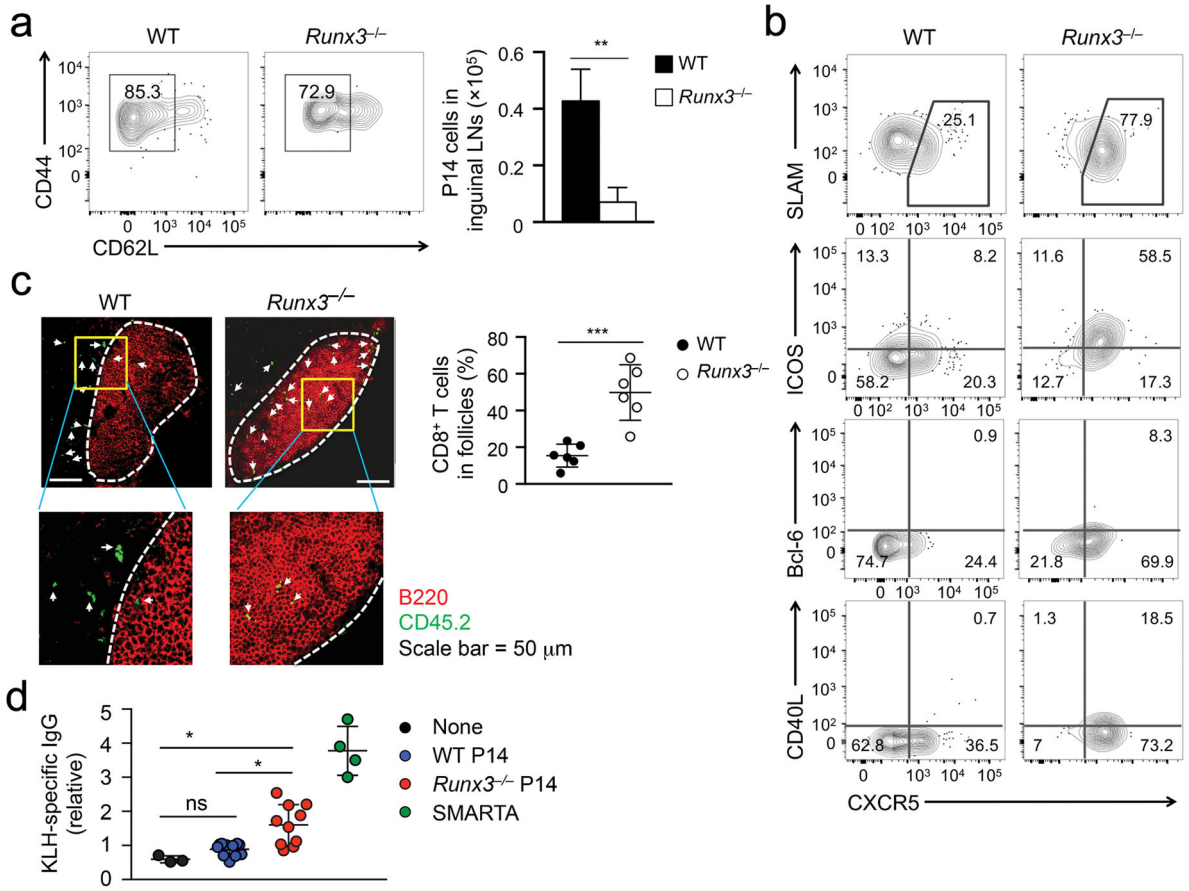

Figure 4. Runx3-deficient CD8$^+$ T_{EFF} cells provide B cell help

(**a**) Activation markers and numbers of WT or *Runx3*$^{-/-}$ P14 CD8$^+$ T_{EFF} cells determined in inguinal LNs on day 7 post-immunization after naïve WT or *Runx3*$^{-/-}$ P14 CD8$^+$ T cells were adoptively transferred into congenic recipients followed by KLH-GP33 immunization. (**b**) Expression of CXCR5, SLAM, ICOS, CD40L and Bcl-6 determined by surface or intracellular staining in WT or *Runx3*$^{-/-}$ P14 T_{EFF} cells on day 7 post-immunization after adoptive transfer and KLH-GP33 immunization. Data are from 2 independent experiments (n = 4–5). (**c**) Immunofluorescence staining of distribution of CD45.2$^+$ WT or *Runx3*$^{-/-}$ P14 T_{EFF} cells (green) in B cell (red) follicles in inguinal LN sections on day 21 after adoptive transfer and KLH-GP33 immunization. Lower panels are 9-fold enlargement of highlighted areas outlined in the main images, and white dotted lines denote the boundary of B cell follicles and T cell zone. The frequency of CD45.2$^+$ cells in B cell follicles among all CD45.2$^+$CD8$^+$ cells in the scanned images is shown in dot plots, with each dot representing one recipient mouse (pooled from 2 independent experiments). ***, p<0.001 (Student's *t*-test). (**d**) Serum KLH-specific IgG measured with ELISA on day 7 post-immunization after CD45.1$^+$*Bcl6*$^{-/-}$ recipient mice were not transferred, or adoptively transferred with 1 × 10^5 sort-purified naïve CD45.2$^+$ WT or *Runx3*$^{-/-}$ P14 CD8$^+$ T cells and then immunized with KLH-GP33. KLH-specific IgG was also determined in another cohort of CD45.1$^+$*Bcl6*$^{-/-}$ mice that were transferred with 1 × 10^5 naïve WT SMARTA CD4$^+$ T cells and then immunized with KLH-GP61. The relative titers at 1:50 dilution, after normalizing to the

average of WT P14 T cell recipient replicates, were pooled from 2–3 independent experiments. Statistical significance for the multi-group comparisons was performed using both unpaired *t*-test and post hoc tests, yielding similar outcomes. ns, not statistically significant; *, $p<0.05$ (Bonferroni's test).

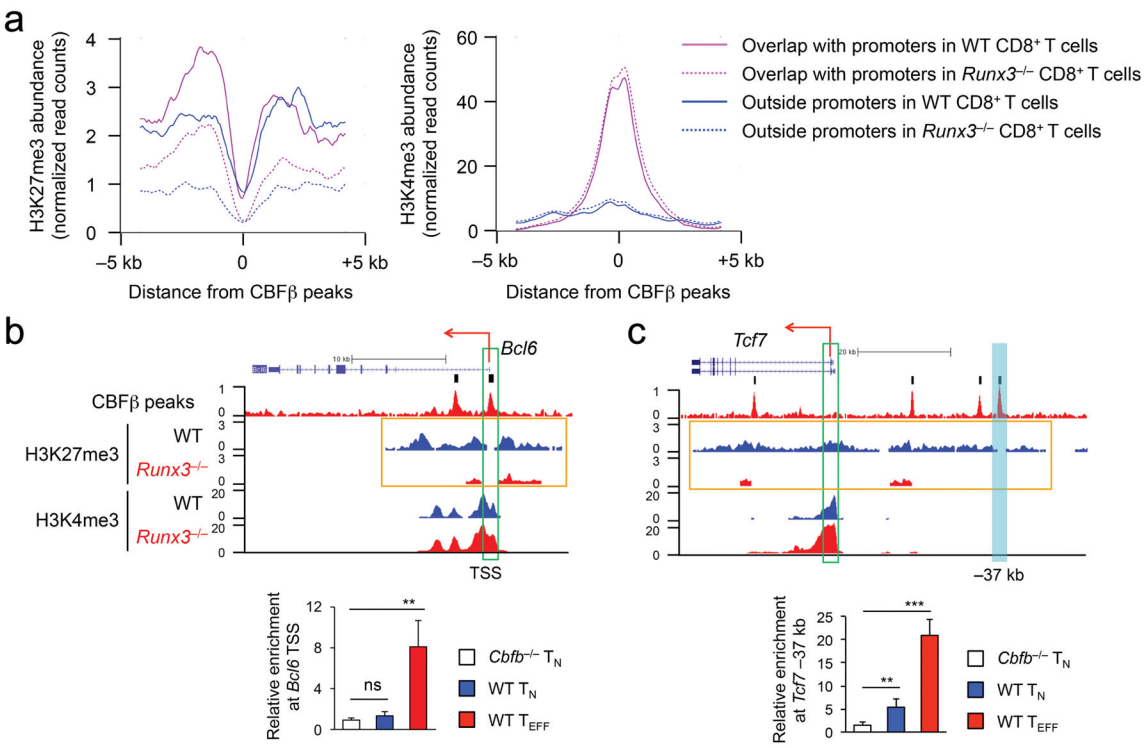

Figure 5. The Runx-CBF complex deploys H3K27me3 to repress T_{FH} genes during CD8$^+$ T_{EFF} cell differentiation

(**a**) The profiles of H3K27me3 (left) and H3K4me3 (right) at CBFβ peaks overlapping with promoters of Runx-CBF-repressed genes (purple lines) or regions outside promoters but within – 5 kb to TES (blue lines) in WT (solid lines) or *Runx3*$^{-/-}$ (dotted lines) P14 CD8$^+$ T_{EFF} cells. CBFβ ChIP-Seq was performed on KLRG1^{hi}IL-7Rα^{lo} P14 CD8$^+$ T_{EFF} cells sort-purified from recipient spleens on day 8 after adoptive transfer of WT P14 CD8$^+$ T cells followed by LCMV-Arm infection, and H3K27me3 and H3K4me3 ChIP-Seq was performed on all CD45.2$^+$ WT or *Runx3*$^{-/-}$ P14 T_{EFF} cells sort-purified from recipient spleens on day 4 after adoptive transfer and LCMV-Arm infection. (**b**–**c**) ChIP-Seq tracks of CBFβ binding peaks and histone modifications at the *Bcl6* (**b**) and *Tcf7* (**c**) gene loci (top panels), with vertical bars on top of CBFβ ChIP-Seq tracks (raw data) denoting the MACS-called high-confidence CBFβ peaks. Green rectangles mark the gene TSS, and orange rectangles highlight the widespread changes in H3K27me3 signals (island-filtered) between WT and *Runx3*$^{-/-}$ P14 T_{EFF} cells. Shown in the bottom panels are relative enrichment of CBFβ binding to the *Bcl6* TSS (**b**) and a *Tcf7* –37 kb regulatory region (cyan filled rectangle, **c**) determined by ChIP-qPCR in *Cbfb*$^{-/-}$ or WT naïve CD8$^+$ T (T_N) cells, or WT P14 T_{EFF} cells sort-purified from recipient spleens on day 5 after adoptive transfer and LCMV-Arm infection. Data are means ± s.d. (n = 4 to 6) from 3 independent experiments. ns, not statistically significant; **, p<0.01; ***, p<0.001 (Student's *t*-test).

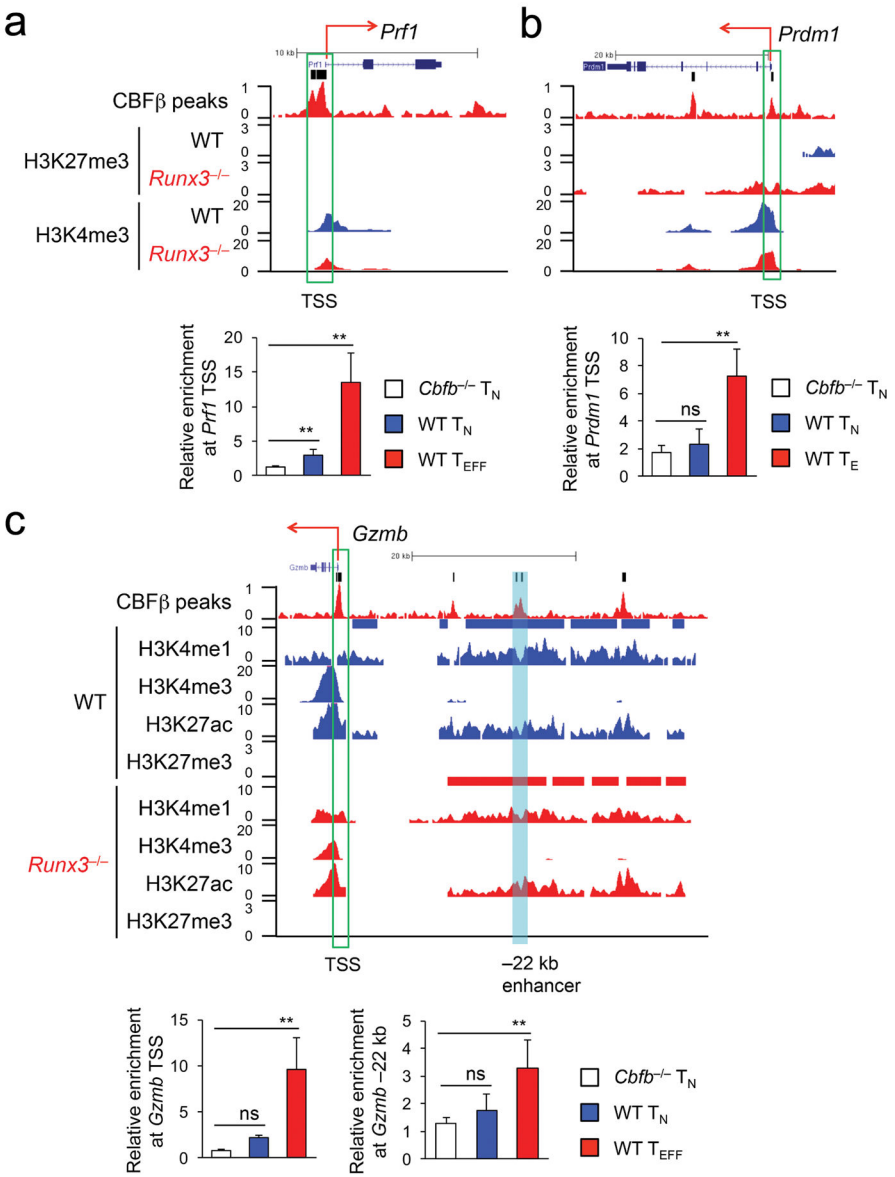

Figure 6. The Runx-CBF complex acts on promoters and enhancers to activate the cytotoxic program during CD8$^+$ T_{EFF} cell differentiation

ChIP-Seq tracks of CBFβ binding peaks and histone modifications at the *Prf1* (**a**), *Prdm1* (**b**) and *Gzmb* (**c**) gene loci (top panels), with vertical bars on top of CBFβ ChIP-Seq tracks (raw data) denoting the MACS-called high-confidence CBFβ peaks and green rectangles marking the gene TSS. In (**c**), a cyan filled rectangle highlights active enhancer upstream of *Gzmb*, and blue and red bars above the H3K4me1 ChIP-Seq tracks (island-filtered) denote active enhancers in WT or *Runx3*$^{-/-}$ P14 CD8$^+$ T_{EFF} cells, respectively. Shown in the bottom panels are relative enrichment of CBFβ binding to the *Prf1* TSS (**a**), *Prdm1* TSS (**b**), and *Gzmb* TSS and a –22 kb upstream enhancer (**c**) determined by ChIP-qPCR in *Cbfb*$^{-/-}$ or WT naïve CD8$^+$ T (T_N) cells, or WT P14 T_{EFF} cells sort-purified from recipient spleens on day 5 after adoptive transfer and LCMV-Arm infection. Data are means ± s.d. (n = 4 to 6)

from 3 independent experiments. ns, not statistically significant; **, $p<0.01$ (Student's *t*-test).

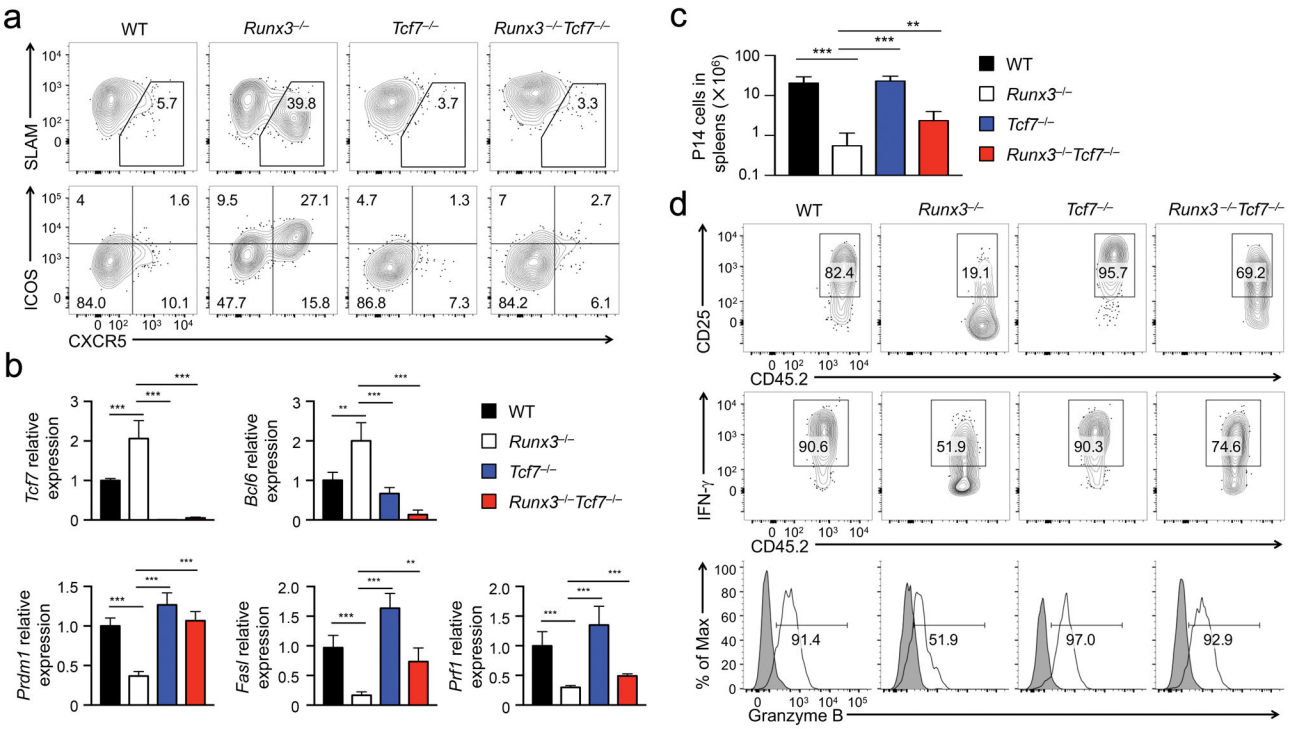

Figure 7. Runx3 represses Tcf1 expression to prevent activation of the T_{FH} program and to assist activation of the cytotoxic program in $CD8^+$ T_{EFF} cells

(**a**) Expression of CXCR5, SLAM and ICOS detected by surface staining on WT, *Runx3*$^{-/-}$, *Tcf7*$^{-/-}$, or *Runx3*$^{-/-}$ *Tcf7*$^{-/-}$ P14 $CD8^+$ T_{EFF} cells in recipient spleens on day 6 after adoptive transfer and LCMV-Arm infection. (**b**) Expression of *Tcf7*, *Bcl6*, *Prdm1*, *Fasl* and *Prf1* genes determined by qRT-PCR in WT, *Runx3*$^{-/-}$, *Tcf7*$^{-/-}$, or *Runx3*$^{-/-}$ *Tcf7*$^{-/-}$ P14 T_{EFF} cells sort-purified from recipient spleens on day 4 after adoptive transfer and LCMV-Arm infection. (**c**) Numbers of WT, *Runx3*$^{-/-}$, *Tcf7*$^{-/-}$, or *Runx3*$^{-/-}$ *Tcf7*$^{-/-}$ P14 T_{EFF} cells determined in recipient spleens on day 6 after LCMV-Arm infection. (**d**) Expression of CD25 and granzyme B, and GP33 peptide-stimulated IFN-γ production determined by surface or intracellular staining in WT, *Runx3*$^{-/-}$, *Tcf7*$^{-/-}$, or *Runx3*$^{-/-}$ *Tcf7*$^{-/-}$ P14 T_{EFF} cells in recipient spleens on day 6 after LCMV-Arm infection. Data are from 2 experiments (n = 4–5), and in **b** and **d**, data are means ± s.d., **, p<0.01; ***, p<0.001 (one-way ANOVA followed by Bonferroni's test).